Chinese Chemical Letters 35 (2024) 108946

Contents lists available at ScienceDirect

Chinese Chemical Letters

journal homepage: www.elsevier.com/locate/cclet

Lysosome-targeted carbon dots with a light-controlled nitric oxide releasing property for enhanced photodynamic therapy

Hao Cai[a,1], Xiaoyan Wu[a,1], Lei Jiang[b], Feng Yu[b], Yuxiang Yang[b], Yan Li[a], Xian Zhang[c], Jian Liu[c], Zijian Li[a,*], Hong Bi[a,*]

[a] School of Materials Science and Engineering, Anhui University, Hefei 230601, China
[b] School of Chemistry and Chemical Engineering, Anhui University, Hefei 230601, China
[c] School of Food and Biological Engineering, Hefei University of Technology, Hefei 230009, China

ARTICLE INFO

Article history:
Received 22 May 2023
Revised 17 August 2023
Accepted 18 August 2023
Available online 19 August 2023

Keywords:
Carbon dots
Nitric oxide
Lysosome-targeting
Photodynamic therapy
Cancer

ABSTRACT

The reactive oxygen species (ROS) generation efficiency is always limited by the extreme tumor microenvironment (TME), leading to unsatisfactory antitumor effects in photodynamic therapy (PDT). As a promising gas therapy molecule, nitric oxide (NO) is independent of oxygen and could even synergize ROS to enhance the therapeutic effect. However, the short half-life, instability, and uncontrollable release of exogenous NO limited the application of tumor synergistic therapy. Herein, we reported a novel kind of red-emissive carbon dots (CDs) that was capable of lysosome-targeted and light-controlled NO delivery. The CDs were synthesized by using metformin and methylene blue (MB) *via* a hydrothermal method. The obtained metformin-MB CDs (MMCDs) exhibited a higher $^1O_2$ quantum yield and NO generation efficiency under light emitting diode (LED) light irradiation. Noteworthily, the $^1O_2$ could further *in situ* oxidize NO into peroxynitrite anions ($ONOO^-$), which own the higher cytotoxicity against cancer cells. Cell experiments indicate that MMCDs could destruct lysosome membrane integrity and kill almost 80% of HepG2 cells under light irradiation while very low cytotoxicity in the dark. Moreover, MMCDs significantly decreased tumor volume and weight after phototherapy in hepatoma HepG2-bearing mice. Our study provides a new strategy for light-controlled NO generation as well as precise lysosome-targeting for enhancement of PDT efficiency.

Related to traditional cancer treatments, photodynamic therapy (PDT) has been increasingly applied in cancer therapy due to its low systemic toxicity, few side effects and negligible drug resistance [1]. Under light irradiation, the photosensitizer would massively transfer O_2 or H_2O into reactive oxygen species (ROS), such as singlet oxygen ($^1O_2$) and hydroxyl radicals ($^{\bullet}OH$), to ablate cancer cells *in situ* [1,2]. However, the extreme tumor microenvironment (TME) restricted the therapeutic potency of PDT. On the one hand, the lower oxygen concentration is often unable to support photosensitizer to generate sufficient ROS; on the other hand, the high glutathione (GSH) level in tumors would neutralize a part of newborn ROS and reduce ROS caused cytotoxicity [3]. Developing new photosensitizers that are independent of the TME is one of the favorable solutions for overcoming these restrictions and enhancing PDT efficiency. Compared with ROS, reactive nitrogen species (RNS) is a nitrogen source free radical that is independent of oxygen supply. RNS mainly refers to nitric oxide (NO) and its derivatives, such as peroxynitrite anions ($ONOO^-$) and peroxynitrous acid (HOONO) [4]. As a promising gas therapy molecule, NO could damage organelles to interfere with the cell energy supply in high doses, which inhibits cellular proliferation, induces apoptosis, and retards cancer metastasis [5]. Importantly, NO would further combine with ROS to generate $ONOO^-$ with great cytotoxicity to tumor cells [6]. Thus, increasing NO donors were developed to cooperate with PDT and improve the antitumor effect [7–9]. L-Arginine is one of the most popular NO donors used in cancer nanomedicine. Related to other NO donors, L-arginine is a natural amino acid with lower toxicity to organisms. The guanidyl of L-arginine would be oxidized to the ureido and produce NO by nitric oxide synthase (NOS) [10]. Although NO donors spontaneously release NO help to neutralize GSH and elevate photo-induced cytotoxicity in PDT, the spontaneously uncontrollable NO-releasing and the inherent short half-life of NO would lead to lower therapeutic efficiency and unpredictable adverse side effects [11,12]. Accordingly, it is of great practical significance to synthesize the novel

* Corresponding authors.
E-mail addresses: 22018@ahu.edu.cn (Z. Li), bihong@ahu.edu.cn (H. Bi).
[1] These authors contributed equally to this work.

https://doi.org/10.1016/j.cclet.2023.108946
1001-8417/

photosensitizer to controllably generate ROS and RNS simultaneously in improving the therapeutic potency of PDT.

Carbon dots (CDs) are fluorescent carbon-based nanomaterials with a size of less than 10 nm and are composed of graphitized sp^2 carbon nuclei and shells containing amino, carboxyl, and hydroxyl groups on the surface [13–15]. Because of their good photoluminescence (PL), high quantum yield (QY), low toxicity, small size and appreciable biocompatibility, CDs have drawn considerable scientific attention in cancer treatments, especially PDT [16–18]. Ge *et al.* first presented a photosensitizer based on CDs that can produce $^1O_2$ *via* a multistate sensitization process, simultaneously allowing imaging and providing efficient cancer therapy [19]. Benefiting from easy surface functionalization modification, CDs were thereby exploited to controllably release NO for enhancing PDT against cancer recently [20]. Photosensitive NO donors were post-modified on the surface of CDs to achieve high controllable NO generation [21]. By light irradiation, photoinduced energy is transferred from the CDs to the modified NO photo-donor, stimulating the NO release [3,22–24]. For instance, Xu *et al.* prepared mitochondria-targeted and NO-releasing CDs in which NO photo-donor was linked on their surface. Under light irradiation, the CDs released NO and cause high cytotoxicity toward the cancer cells by specifically damaging their mitochondria [24]. Fang *et al.* located CDs in the band gap of graphitic carbon nitride, and then poly-L-arginine was coupled to the surface carboxyl group to obtain the poly-L-arginine modified carbon-dots-doped graphitic carbon nitride nanomaterial (ArgCCN). Under red laser irradiation, 200 μg/mL ArgCCN would gradually increase NO concentration to 16 μmol/L within 30 min and inhibited about 60% of cancer cell viability [3]. However, the multiple assembly and post-modification would reduce the load capacity of the NO donor in CDs. In addition, chemical bonding between CDs and NO donors may consume some NO-producing groups, which further lowers the NO generation efficiency. Therefore, it is essential to explore more efficient NO photo-donors and improve the CD synthesis strategy in NO-related cancer phototherapy.

As the stomach of cells, lysosomes play critical roles in many physiological processes and contain more than 60 acid hydrolases that could break down cellular components and complex macromolecules into their constituent structural units [25,26]. Hence, the lysosome is an effective therapeutic target to melt tumors. The cancer cells would start the suicide procedure rapidly after the structure and permeability of the lysosome are disrupted [27,28]. In PDT, the development of a photosensitizer that specifically delivers NO to lysosomes is expected to obtain maximal therapeutic efficacy and minimal side effects.

Metformin, a potential drug for tumor therapy, has been introduced to participate in CD synthesis in recent years [29–31]. Herein, inspired by the NO generation process from the guanidyl of L-arginine, metformin which possessed double guanidyl was exploited to be modified on the surface of CDs to acquire a high yield of NO under light irradiation. We proposed a novel photo-controlled NO-releasing CD based on an intrinsic core-shell structure that can efficiently generate ROS/RNS in the cancer PDT (Scheme 1). The CDs were synthesized by using methylene blue (MB) and metformin *via* hydrothermal strategy. The as-synthesized metformin-MB CDs (MMCDs) had red fluorescence emission and can be located in the lysosomes of the cancer cells. Under light irradiation, the MMCDs would boost amounts of $^1O_2$ and NO to form $ONOO^-$ and subsequently damaged the structure and permeability of the lysosome, which accelerated cancer cell death (Scheme 1). These studies suggested an emerging lysosome-targeted and light-controlled NO-releasing CD that has a promising application in cancer phototherapy.

As shown in the transmission electron microscopy (TEM) image, MMCDs were well-dispersed and spherical particles with an

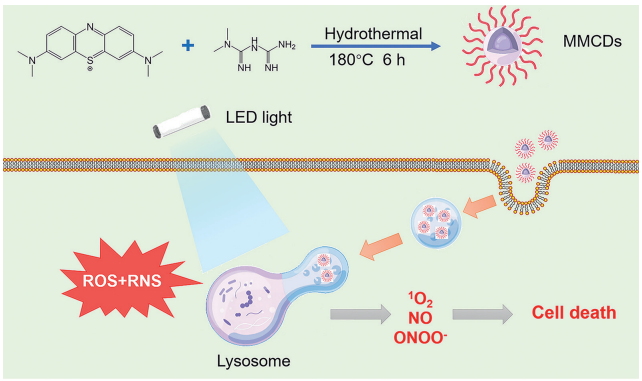

Scheme 1. Schematic illustration of the preparation of MMCDs and the underlying mechanism of tumor cell death induced by photodynamic lysosomal impairment.

average size of 2.88 nm (Fig. 1a). The high-resolution TEM image displayed that MMCDs had a lattice spacing of 0.21 nm (Fig. 1a), which was consistent with the graphite (100) crystal plane [32]. The atomic force microscopy (AFM) image further showed the height profile of MMCDs ranging from 0.74 nm to 1.62 nm (Fig. 1b). Subsequently, X-ray powder diffraction (XRD) pattern found that MMCDs had a broad (002) peak centered at 22° (Fig. 1c), suggesting a better crystallinity of the carbon core. Moreover, the Raman spectrum had two peaks at 1409 cm^{-1} (disordered D band) and 1579 cm^{-1} (crystalline G band), with a D to G intensity ratio (I_D/I_G) of 0.72 (Fig. 1d). Concomitantly, the emergence of A band suggested the existence of five or seven-membered rings in MMCDs, which may arise from the N-doping effect (Fig. 1d) [33]. These

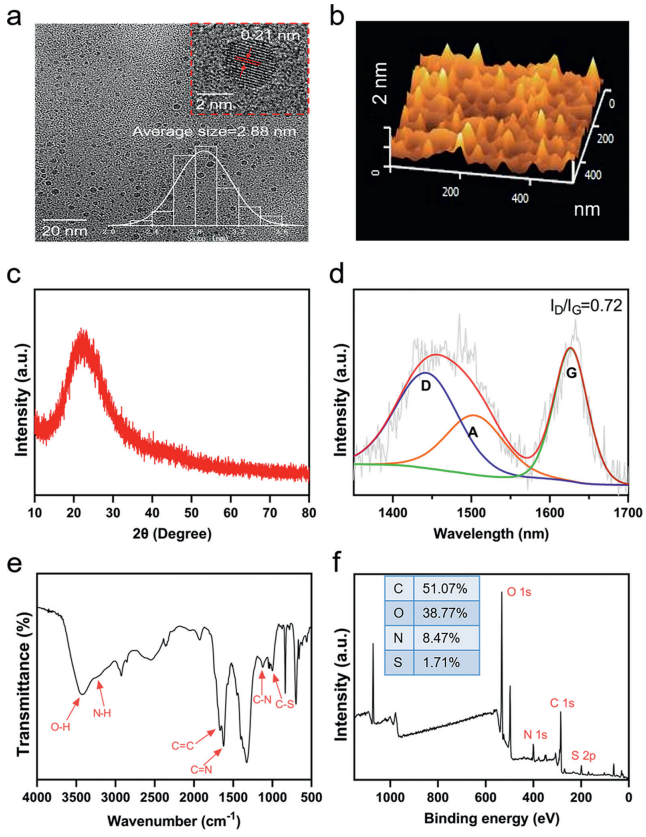

Fig. 1. (a) TEM image and its high-resolution TEM image of MMCDs, the inset shows the size distribution of MMCDs. (b) AFM image, (c) XRD pattern, (d) Raman spectrum, and (e) FT-IR spectrum of MMCDs. (f) XPS survey spectrum of MMCDs, the inset shows the atomic ratio of each element.

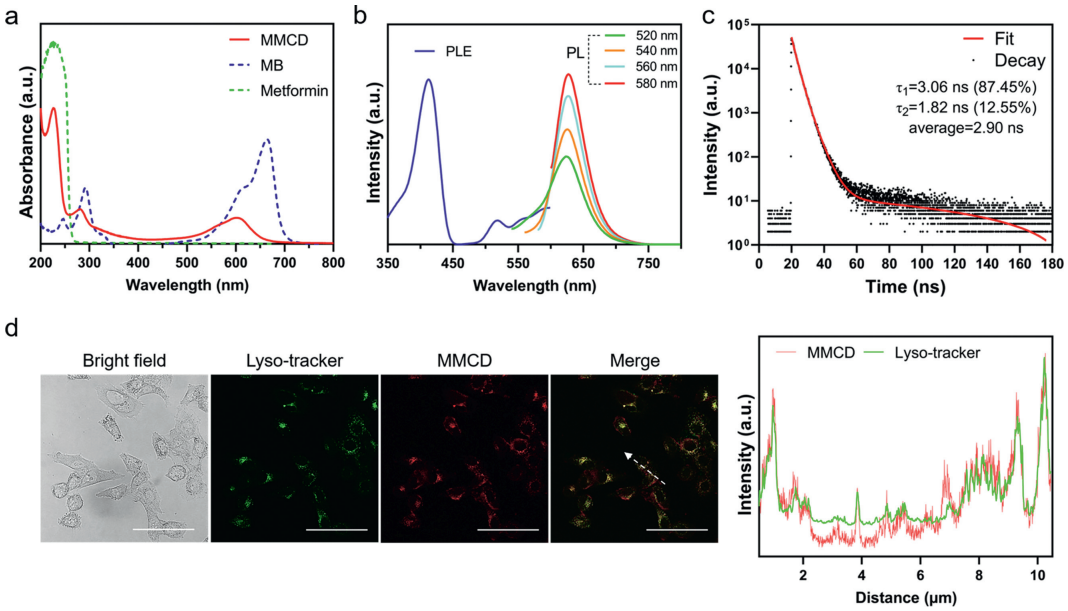

Fig. 2. (a) Ultraviolet–visible (UV–vis) absorption. (b) PL and PLE spectra of MMCDs. (c) Photoluminescence decay trace of MMCDs recorded at 627 nm. (d) CLSM of HepG2 cells stained with Lyso-tracker after incubation with MMCDs and its fluorescence intensity curves between the green and red channels, scale bar = 50 μm.

results indicated the coexistence of graphitic and amorphous carbons in MMCDs.

We following detected the chemical compositions of MMCDs. Fourier transform infrared (FT-IR) spectra preliminarily detected the stretching vibration bands of O-H (3400 cm^{-1}), N-H (3212 cm^{-1}), C=C (1673 cm^{-1}), C=N (1627 cm^{-1}), C–N (1125 cm^{-1}), C-S (995 cm^{-1}) in MMCDs (Fig. 1e). And then, X-ray photoelectron spectroscopy (XPS) was performed to achieve more powerful evidence. Screening the full XPS spectra indicated that MMCDs mainly consist of C, O, N, and S elements with atomic contents of 51.07%, 38.77%, 8.47%, and 1.71%, respectively (Fig. 1f). The high-resolution XPS spectrum of C 1s can be deconvoluted into four components corresponding to C=C/C-C (284.80 eV), C-O/C-N/C-S (285.70 eV), C=O/C=N (288.65 eV), and -CO_3 (290.00 eV) (Fig. S1a in Supporting information) [34,35], while C–O (532.90 eV) and C=O (531.75 eV) were presented in the O 1s band (Fig. S1b in Supporting information). The high atomic ratio of O may be due to the generation of oxygen-containing groups (–OH and –COOH) during the hydrothermal reaction. Moreover, the spectrum of N 1s can be deconvoluted into three peaks at 398.95, 400.05 and 400.85 eV, which were attributed to the pyridinic N, pyrrolic N, and graphitic N, respectively (Fig. S1c in Supporting information). In particular, the high-resolution XPS spectrum of S 2p was deconvoluted into four components, including C-S $2p_{3/2}$ (163.60 eV), C-S $2p_{1/2}$ (164.95 eV), C-SO_2–C (168.80 eV), and -SO_3 (170.15 eV) (Fig. S1d in Supporting information) [35]. According to these results, we inferred that metformin was involved in the formation of ring structures in MMCDs and part of the S-containing six-membered ring from MB was opened to bound O to present different valence states. Since the aromatic structure and easy polymerization, MB was supposed to play a central role in the promotion of the graphitization process and formation of the carbon core of MMCDs [36,37]. To verify this hypothesis, we adopted nuclear magnetic resonance (NMR) spectroscopy to investigate surface groups of MMCDs and their precursors. The ^{1}H NMR resonances located in the range of 6.7–7.6 ppm could be ascribed to guanidine protons in metformin (Fig. S2 in Supporting information). Meanwhile, the ^{1}H NMR resonance at 2.87 ppm can be assignable to N-methyl protons from metformin (Fig. S2). Meanwhile, control CDs with a single precursor were also synthesized. Interestingly, CDs could not be synthesized with metformin as a single precursor while a large number of CDs can be obtained with MB as the only precursor. The MB-derived CDs (MBCDs) exhibited well crystallinity of the carbon core as shown in the XRD pattern (Fig. S3a in Supporting information). Thus, we speculated that MMCDs have a core-shell structure, where the carbon core is mainly composed of MB-derived π-conjugated domains and the shell is decorated with abundant guanidyl left by metformin.

Next, the optical properties of MMCDs were evaluated. Owing to the interplay of chromophores in the carbon core and functional groups on the surface, MMCDs show extensive absorption from ultraviolet (UV) to the red-light region in an aqueous solution (Fig. 2a). The main UV absorption peak centered at 226 nm could be assigned to the π-π^* transition of surface metformin moieties. Moreover, the broadband in the lower energy range from 280 nm to 700 nm (λ_{abs} = 600 nm) may be derived from the absorption of MB units in the carbon core, which was similar to the MBCDs (Fig. 2a and Fig. S3b in Supporting information). These assignments agree well with the absorption profiles of the precursors, suggesting the precursor structural features were retained in MMCDs. The photoluminescence excitation (PLE) spectrum showed major contributions from the visible light region (Fig. 2b). Visible light excitation of MMCDs showed strong red fluorescence (λ_{max} = 642 nm) in aqueous solution as MBCDs like and the emission maximum was independent of the excitation wavelength (λ_{ex} = 520–580 nm), indicative of its origin from an internal emission center (Fig. 2b and Fig. S3b). In addition, the emission quantum yield (Φ_{em}) of MMCDs in an aqueous solution was 7.11% with an average fluorescence lifetime of 2.90 ns (Fig. 2c). The lifetime value falls in the nanosecond range, suggesting the singlet excited state of the MMCDs. The fluorescence decay curve of MMCDs can be divided into a slow component (τ_1 = 3.06 ns) and a fast component (τ_2 = 1.82 ns), which indicates that both the carbon core and surface state have contributed to the red emission of MMCDs [38].

To evaluate the photostability of MMCDs, we then detected the fluorescence intensity in different pH, solutions, temperatures and days. The results showed that MMCDs exhibited high stability in various physiological media, including water, saline, phosphate-buffered solution (PBS), Dulbecco's modified Eagle's medium (DMEM) and Roswell Park Memorial Institute (RPMI) 1640 medium (Fig. S4a in Supporting information). Similar observations were also demonstrated in various pH, temperatures and days

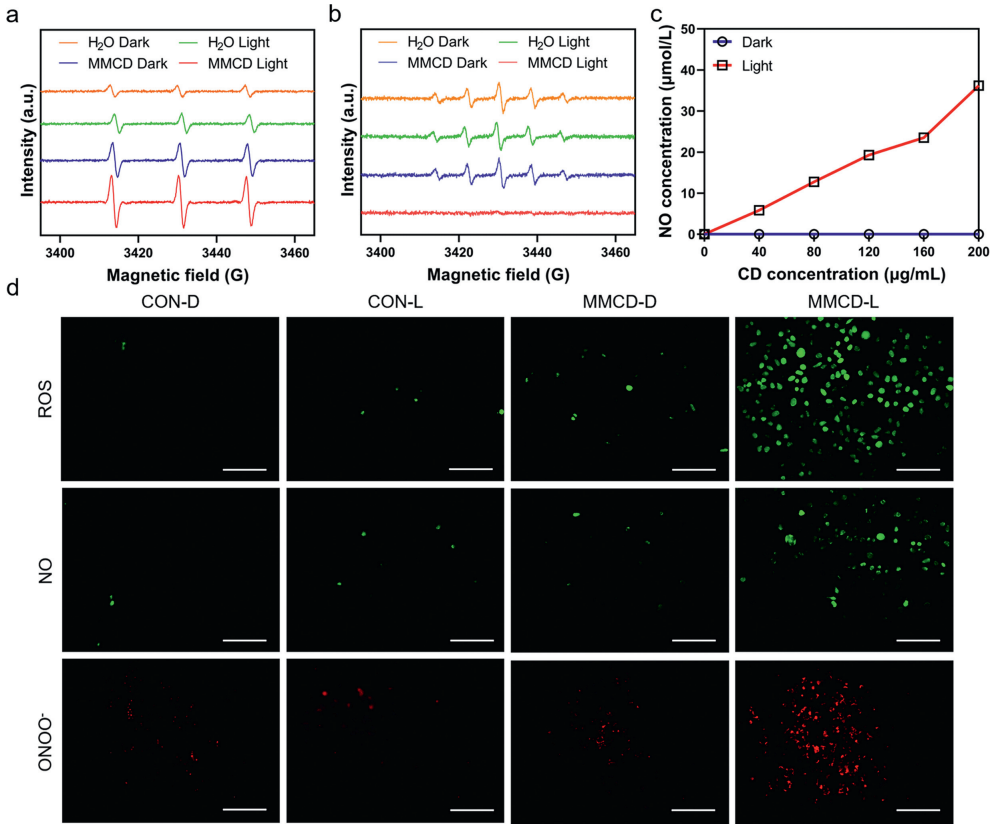

Fig. 3. (a) EPR spectra of TEMP trapping the $^1O_2$ and (b) EPR spectra of PTIO trapping the NO produced by MMCDs under LED irradiation (400–500 nm, 100 mW/cm^2, 5 min). (c) NO generation in the presence of different MMCD concentrations. (d) Fluorescence images of HepG2 cells labeled with ROS, NO and ONOO$^-$ probes after irradiating with LED light (400–500 nm, 100 mW/cm^2) for 12 min, scale bar = 100 μm.

(Figs. S4b–d in Supporting information). After determining the optical properties, the intracellular distribution of MMCDs was explored in the cancer cells. As shown in confocal laser scanning microscopy (CLSM), HepG2 cells incubated with MMCDs presented red fluorescence and were highly consistent with the location of commercial lysosome probe (Lyso-Tracker Green) but not mitochondria probe (Mito-tracker) or endoplasmic reticulum probe (ER-tracker) (Fig. 2d and Fig. S5 in Supporting information). Color-dependent pixel intensity curves showed high Pearson's coefficients (0.81) which revealed the lysosome-targeting capability of MMCDs (Fig. 2d). Since the lysosome membrane potential was +114 mV [39], the binding of MMCDs to lysosome was related to negative zeta potential (−28.1 mV). The negative potential was associated with a high atomic ratio of O in MMCDs, which attribute to abundant negatively charged oxygen-containing groups (–OH and –COOH) on the surface.

Furthermore, the ability of MMCDs as photosensitizers was investigated. As analyzed from the electron paramagnetic resonance (EPR) spectrum, paramagnetic signals of $^1O_2$ but not $^{\bullet}OH$ emerge upon photoexcitation of MMCDs in the presence of specific ROS trapping agents (2,2,6,6-tetramethylpiperidine (TEMP) for $^1O_2$ and 5,5-dimethylpyrroline *N*-oxide (DMPO) for $^{\bullet}OH$) (Fig. 3a and Fig. S6a in Supporting information). Meanwhile, the $^1O_2$ paramagnetic signal comparison of MMCDs and MBCDs indicated that metformin left in the shell of MMCDs did not influence the ROS generation of MB-derived carbon core (Fig. S6b in Supporting information). The $^1O_2$ QY was subsequently evaluated using water-soluble 9,10-anthracenediacyl-bis(methylene)malonic acid (ABDA) assay and rose bengal (RB) was performed as a standard photosensitizer [35,40]. By monitoring the absorption of ABDA at 378 nm in different irradiation times, the $^1O_2$ QY was determined to be 78.36% which was even higher than RB (Fig. S7 in Supporting information). These outcomes suggested an excellent $^1O_2$ generate efficiency of MMCDs. Notably, the EPR spectrum also found the paramagnetic signal of MMCDs was changed after light irradiation in the presence of NO special trapping agent 2-phenyl-4,4,5,5-tetramethylimidazoline-1-oxyl-3-oxide (PTIO), which EPR signal would be appeased when it captured NO free radicals (Fig. 3b). To quantitative analyze NO generation, we examined NO concentration in various MMCD concentration after 5 min light emitting diode (LED) irradiation. With the increase of MMCD concentration, the NO generation was increased to 35 μmol/L when the concentration of MMCDs reached 200 μg/mL and each mg MMCD can be calculated to produce 0.175 μmol NO (Fig. 3c). The generation of ROS and RNS were detected in cancer cells as well. It was obviously found that the HepG2 cells treated with MMCDs under light irradiation had more positive ROS and NO fluorescence proportion than their control (Fig. 3d). Additionally, in view of ROS would further transform NO to ONOO$^-$ which has more cytotoxicity than NO and $^1O_2$ [6,41]. The ONOO- probe was introduced to detect the generation of ONOO$^-$. As expected, MMCDs boosted ONOO$^-$ production under light irradiation in HepG2 cells (Fig. 3d). Collectively, these results suggested the application potential of MMCDs in PDT by collaborating NO and $^1O_2$ to generate ONOO$^-$ in cancer cells.

Hence, the cytotoxicity of MMCDs under light irradiation was assessed. The MMCDs were primarily incubated with human normal hepatocyte QSG7701 and cancer cell HepG2, respectively. The results showed that MMCDs had very low cytotoxicity from 0 to 200 μg/mL in the dark which suggested great biosecurity without light irradiation (Fig. 4a). Besides, in the range of the above concentration, MMCDs also exhibited higher biosecurity and biocompatibility in the hemolysis assay (Fig. S8 in Supporting information). However, after 12 min LED irradiation (100 mW/cm^2), the cell viability of HepG2 cells sharply decreased to about 20%

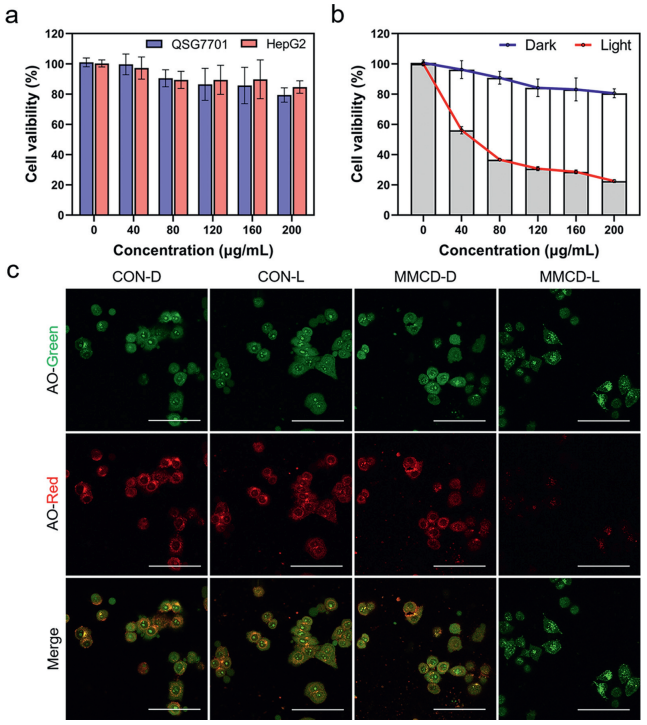

Fig. 4. (a) Cell viability of different cells incubated with MMCDs at different concentrations. (b) Cell viability of HepG2 cells incubated with different concentrations of MMCDs under dark and light conditions (LED, 400–500 nm, 100 mW/cm^2) for 12 min. (c) AO staining of HepG2 cells treated with MMCDs under dark or LED light irradiation (400–500 nm, 100 mW/cm^2) for 12 min, scale bar = 50 μm. Data are presented as mean ± standard deviation (SD) of 6 samples per group, two-tailed Student's *t*-test.

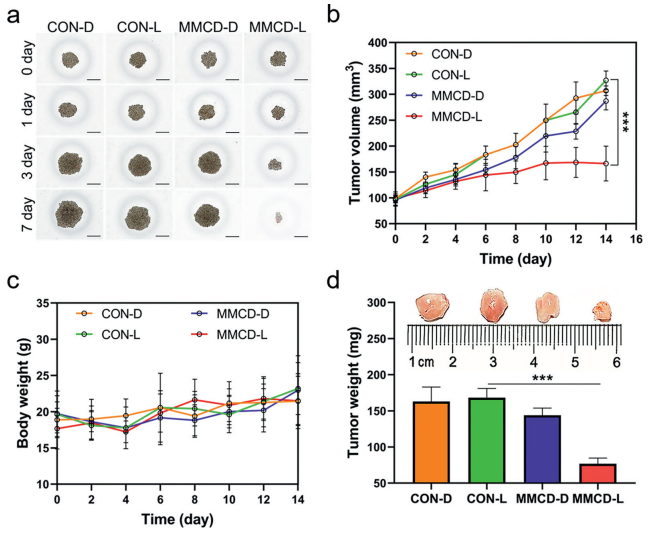

Fig. 5. (a) Images of HepG2 3D MCs co-incubated with PBS and MMCDs. These images were captured daily under dark or LED light irradiation (400–500 nm, 100 mW/cm^2, 12 min), scale bar = 200 μm. (b) Tumor volume of HepG2-tumor-bearing nude mice. (c) Body weight changes during the PDT. (d) Tumor photos and weights of mice from different groups after PDT. Data are presented as mean ± SD of 5 mice per group, one-way ANOVA with Mann–Whitney test; $^{***}P < 0.001$.

when the MMCD concentration was 200 μg/mL (Fig. 4b), demonstrating the excellent ability of MMCD as a PDT agent. The results were further confirmed by the calcein-acetoxymethyl ester/propidium iodide (calcein-AM/PI) assay, in which living cells would be stained with green fluorescence coming from calcein-AM while dead cells presented red fluorescence from PI. As it is shown in fluorescence images, the cells treated with 200 μg/mL MMCDs had higher cytotoxicity under light irradiation than their dark control (Fig. S9 in Supporting information). The underlying mechanism of cell death was explored as well. Given intracellular MMCDs were highly enriched in lysosomes, we introduced acridine orange (AO) to investigate the permeability and integrity of lysosomes in cancer cells. AO would display bright red fluorescence in the acidic microenvironment of the lysosome. Our results showed that the cells incubated with MMCDs and undergoing light irradiation had lower red fluorescence intensity related to the cells without illumination or MMCDs treatment (Fig. 4c), suggesting impaired lysosome structure and permeability.

Finally, to evaluate the antitumor activity of MMCDs, a 3D multicellular spheroid (3D MCs) model was primarily established to simulate the dynamic change of tumors under physiological conditions [42,43]. Consistent with the therapeutic effect in cells, the size of 3D MCs was not reduced after 7 days in the absence of MMCDs or light. However, the volume of 3D MCs with phototherapy was significantly decreased with the prolongation of MMCD incubation time (Fig. 5a). Subsequently, the tumor-bearing mouse model was established on a xenograft nude mouse with HepG2 cells. Animal welfare and experimental procedures were strictly examined and approved by the Animal Ethics Committee of Anhui University. The mice would receive light irradiation when the tumor volume reached 100 mm^3. After two weeks, it can be found that the volume of tumors was significantly inhibited by MMCD treatment under light irradiation (Fig. 5b). Meanwhile, no body weight loss occurred over the duration of treatments, revealing negligible toxicity of MMCDs (Fig. 5c). Accompany with the inhibition of tumor growth, MMCD treatment also reduced the tumor weight after PDT (Fig. 5d). Thus, MMCDs was affirmed to process an antitumor effect *in vivo* for translational medicine potential.

In conclusion, we successfully designed and synthesized a novel light-controlled NO-releasing nanoplatform for lysosome-targeted PDT in tumors. The MMCDs were prepared from MB and metformin through a facile bottom-up approach and precursor structural features were well retained. The carbon core was mainly composed of MB-derived π-conjugated domains and amounts of guanidyls left from metformin were modified on its surface. On account of the fluorescent and photodynamic properties of MB, MMCDs presented red fluorescence and well ROS generation efficiency. Additionally, the double guanidine left on the surface of MMCDs could be oxidized and release massive NO, which had great efficiency and would subsequently transform into $ONOO^-$ with stronger cytotoxicity. In cell experiments, our results showed that MMCDs could be highly enriched in the lysosome and "turned on" enormous ROS/RNS production mode to ablate cancer cells under light irradiation while it had great biosecurity and biocompatibility in the dark. *In vivo*, MMCDs also decreased tumor volume and weight after phototherapy in hepatoma HepG2-bearing mice. Mechanically, it was found that MMCDs located in lysosomes would disrupt the structure and permeability of the lysosome, which suggested the leak of massive acid hydrolases that could break down cellular components into their constituent structural units. Collectively, our studies provided a promising strategy for light-controlled powerful ROS/RNS generation in enhancing PDT efficiency and offered a new insight for exploiting NO precise organelle targeting in cancer therapy.

Declaration of competing interest

The authors declare that they have no known competing financial interests or personal relationships that could have appeared to influence the work reported in this paper.

Acknowledgments

This work was financially supported by the National Natural Science Foundation of China (Nos. 52172033 and 22005280). We acknowledge the support from the support of the Key Laboratory of Structure and Functional Regulation of Hybrid Materials of the Ministry of Education, Anhui University, China. The authors also acknowledge the support from the Key Laboratory of Environment Friendly Polymer Materials of Anhui Province, China, and Key Laboratory of Functional Inorganic Material Chemistry of Anhui Province, Anhui University, China. The graphic abstract and scheme were supported by Figdraw.

Supplementary materials

Supplementary material associated with this article can be found, in the online version, at doi:10.1016/j.cclet.2023.108946.

References

[1] D.E. Dolmans, D. Fukumura, R.K. Jain, Nat. Rev. Cancer 3 (2003) 380–387.
[2] M. Lan, S. Zhao, W. Liu, et al., Adv. Healthc. Mater. 8 (2019) e1900132.
[3] X. Fang, S. Cai, M. Wang, et al., Angew. Chem. Int. Ed. 60 (2021) 7046–7050.
[4] Y. Zhao, X. Ouyang, Y. Peng, S. Peng, Pharmaceutics 13 (2021) 1917.
[5] V. Somasundaram, D. Basudhar, G. Bharadwaj, et al., Antioxid. Redox Signal. 30 (2019) 1124–1143.
[6] H.J. Forman, H. Zhang, Nat. Rev. Drug Discov. 20 (2021) 689–709.
[7] Y. Deng, F. Jia, S. Chen, et al., Biomaterials 187 (2018) 55–65.
[8] M.D. Lu, X. Zhou, Y.J. Yu, et al., Chin. Chem. Lett. 24 (2013) 415–418.
[9] L. Wang, K. Kang, Y. Ma, et al., Chem. Eng. J. 444 (2022) 136512.
[10] M. Wang, Z. Hou, S. Liu, et al., Small 17 (2021) e2005728.
[11] Z. Yuan, C. Lin, Y. He, et al., ACS Nano 14 (2020) 3546–3562.
[12] F.H. Khan, E. Dervan, D.D. Bhattacharyya, et al., Int. J. Mol. Sci. 21 (2020) 9393.
[13] L. Ethordevic, F. Arcudi, M. Cacioppo, M. Prato, Nat. Nanotechnol. 17 (2022) 112–130.
[14] H. Cai, K. Abbas, Y. Yang, Z. Li, H. Bi, Appl. Res. 2 (2023) e202300001.
[15] B. Wang, Z. Wei, L. Sui, et al., Light Sci. Appl. 11 (2022) 172.
[16] B. Wang, H. Cai, G.I.N. Waterhouse, et al., Small Sci. 2 (2022) 2200012.
[17] B. Wang, G.I.N. Waterhouse, S. Lu, Trends Chem. 5 (2023) 76–87.
[18] X. Yang, X. Li, B. Wang, et al., Chin. Chem. Lett. 33 (2022) 613–625.
[19] J. Ge, M. Lan, B. Zhou, et al., Nat. Commun. 5 (2014) 4596.
[20] C. Han, X. Zhang, F. Wang, et al., Carbon 183 (2021) 789–808.
[21] Q. Deng, H. Xiang, W. Tang, et al., J. Inorg. Biochem. 165 (2016) 152–158.
[22] C. Fowley, A.P. McHale, B. McCaughan, et al., Chem. Commun. 51 (2015) 81–84.
[23] R. Gui, A. Wan, Y. Zhang, H. Li, T. Zhao, RSC Adv. 4 (2014) 30129–30136.
[24] J. Xu, F. Zeng, H. Wu, et al., Small 10 (2014) 3750–3760.
[25] S.R. Bonam, F. Wang, S. Muller, Nat. Rev. Drug Discov. 18 (2019) 923–948.
[26] S. Zhao, S. Wu, Q. Jia, et al., Chem. Eng. J. 388 (2020) 124212.
[27] Y. Li, H. Jia, H. Wang, et al., J. Control. Release 351 (2022) 692–702.
[28] Y. Xiao, X. Yin, P. Sun, et al., Chin. Chem. Lett. 33 (2022) 5051–5055.
[29] H. Yao, S. Zhang, X. Guo, et al., Nanomedicine 20 (2019) 101978.
[30] J. Wan, S. Xu, J. Li, et al., Nanoscale 14 (2022) 11359–11368.
[31] L. Yu, Y. Wang, K. Li, et al., Carbon 212 (2023) 118095.
[32] X. Tian, X. Yin, Small 15 (2019) e1901803.
[33] M.W. Smith, I. Dallmeyer, T.J. Johnson, et al., Carbon 100 (2016) 678–692.
[34] Q. Luo, H. Ding, X. Hu, et al., Dalton Trans. 49 (2020) 6950–6956.
[35] X. Hu, S. Wang, Q. Luo, et al., Chin. Chem. Lett. 32 (2021) 2287–2291.
[36] Y. Xu, C. Wang, G. Ran, et al., ACS Appl. Nano Mater. 4 (2021) 4820–4828.
[37] N. Xu, Q. Gu, J. Du, et al., Sci. China Mater. 64 (2021) 2325–2336.
[38] B. Wang, H. Song, Z. Tang, B. Yang, S. Lu, Nano Res. 15 (2022) 942–949.
[39] A. Saminathan, J. Devany, A.T. Veetil, et al., Nat. Nanotechnol. 16 (2021) 96–103.
[40] Q. Liang, F. Yu, H. Cai, et al., J. Mater. Chem. B 11 (2023) 2466–2477.
[41] Y. Chen, Z. Li, P. Pan, R. Zeng, X. Zhang, ACS Nano 15 (2021) 11514–11525.
[42] L.P. Ferreira, V.M. Gaspar, J.F. Mano, Biomaterials 185 (2018) 155–173.
[43] J. Karges, T. Yempala, M. Tharaud, D. Gibson, G. Gasser, Angew. Chem. Int. Ed. 59 (2020) 7069–7075.